Macromolecules

Article

Cite This: Macromolecules 2020, 53, 302−311

pubs.acs.org/Macromolecules

Decoupling the Polymer Dynamics and the Nanoparticle Network Dynamics of Polymer Nanocomposites through Dielectric Spectroscopy and Rheology

Jie Yang,[†,‡] Matthew Melton,[‡] Ruikun Sun,[‡] Wei Yang,*[,†] and Shiwang Cheng*[,‡]

[†]College of Polymer Science and Engineering, State Key Laboratory of Polymer Materials Engineering, Sichuan University, Chengdu, Sichuan 610065, People's Republic of China

[‡]Department of Chemical Engineering and Materials Science, Michigan State University, East Lansing, Michigan 48824, United States

ABSTRACT: The dynamics of polymer nanocomposites (PNCs) are dictated by two intertwining components, the polymer matrix and the nanoparticle network, whose characteristics have not been elucidated. Here, we unravel the salient features of the polymer matrix dynamics and the nanoparticle network dynamics through dielectric spectroscopy and rheology. Dielectric measurements show that the dynamics of the polymer matrix of PNCs are almost identical to that of the neat polymer. In contrast, rheological measurements exhibit a strong deviation in the dynamics of PNCs from that of the neat polymer. Detailed analyses show that the rheology captures both contributions of the polymer matrix and the nanoparticle network while dielectric measurements are only sensitive to polymer matrix dynamics. Moreover, the dynamics of the polymer matrix and the nanoparticle network have very different temperature dependences, leading to a dynamic decoupling phenomenon and the breakdown of the time−temperature superposition principle in PNCs.

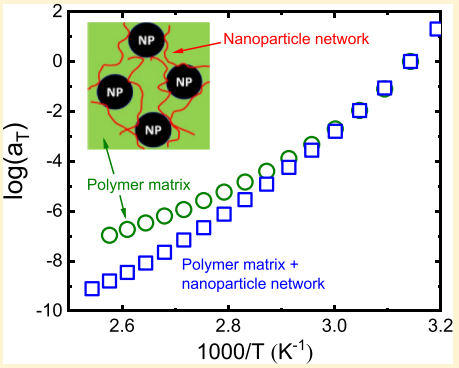

1. INTRODUCTION

Polymer nanocomposites (PNCs) are widely used as structural and functional materials due to their light weight, low cost, high mechanical strength, and good compatibility.[1−6] The design and application of PNCs rely heavily on their dynamic and mechanical properties.[1,2,6−8] Master curves of the dynamic moduli of PNCs have usually been constructed through the time−temperature superposition principle (TTSP),[9−11] where the rheological shift factor, a_T^R, represents the change in polymer dynamics with temperature. The a_T^R also sets the foundation for the PNC processing, design, and performance evaluation. For PNCs at high nanoparticle loadings, the a_T^R typically shows much stronger temperature dependence than the neat polymer.[9,10] Alternatively, polymer dynamics of PNCs measured by selective methods such as the broadband dielectric spectroscopy (BDS), a_T^B (the dielectric shift factor), usually show identical Williams−Landel−Ferry (WLF) temperature dependence as the neat polymer, regardless of the loading of nanoparticles.[12−15] Thus, it is important to understand the discrepancies in the polymer dynamics of PNCs, the a_T^R and a_T^B, from different techniques.

The thermomechanical properties of PNCs are known to correlate with the two intertwining components: the polymer matrix network and the nanoparticle network.[6,10,16−22] For PNCs with well-dispersed nanoparticles, the nanoparticle network forms through polymer bridging. Quan et al.[16] demonstrated that the linear viscoelastic spectra of PNCs with well-dispersed nanoparticles could be quantitatively described by taking into account the gel dynamics of the nanoparticle network, emphasizing the critical role of the nanoparticle network. Baeza et al.[10] observed a change in the a_T^R from a WLF to an Arrhenius temperature dependence for PNCs at high loadings, which was also attributed to the nanoparticle network dynamics. Although the critical roles of the nanoparticle network have been heavily emphasized recently, the nanoparticle network dynamics remain largely unexplored.

In this article, we decouple the polymer dynamics and the nanoparticle network dynamics of PNCs through a combination of BDS and rheology. Specifically, BDS measurements demonstrate identical temperature dependence in the dynamics of the PNCs and the neat polymer, a_T^B, regardless of the loading of nanoparticles. In contrast, small amplitude oscillatory shear (SAOS) and creep measurements of the same PNCs clearly show difference in the a_T^R between PNCs and the neat polymer. Moreover, the TTSP is only valid for PNCs at low loadings in the absence of the nanoparticle network, and a breakdown of the TTSP takes place at high nanoparticle loadings when the nanoparticle network emerges. In addition, we demonstrate that large strain predeformation followed by linear viscoelastic measurements can be an effective way of separating the dynamics of the polymer matrix

Received: July 29, 2019
Revised: November 4, 2019
Published: December 31, 2019

DOI: 10.1021/acs.macromol.9b01584
Macromolecules 2020, 53, 302−311

and the nanoparticle network. Interestingly, the a_T^R of PNCs with predeformation deviates significantly from that in the absence of predeformation and follows identical temperature dependence with the a_T^B. We conclude that the a_T^R of PNCs contains the contributions from both the polymer matrix and the nanoparticle network, while the BDS only measures the dynamics of the polymer matrix. Furthermore, it is the dynamics of the nanoparticle network that lead to the difference between the a_T^R and the a_T^B as well as the failure of the TTSP of PNCs at high nanoparticle loadings.

2. MATERIALS AND METHODS

2.1. Materials. Two polymers, poly(vinyl acetate) (PVAc) and polypropylene glycol (PPG), and two types of SiO_2 nanoparticles with a radius of R_{NP} = 7 ± 2 nm (Nissan Chemical, MEK-AC2140Z) and R_{NP} = 12.5 ± 2.5 nm (synthesized by a modified Stöber's method[23,24] in ethanol at a concentration of 15 mg/mL), are included in this study. The PVAc (Spectrum Chemical MFT Corp.) has a molecular weight (M_W) of 40 kg/mol and a polydispersity index (PDI) of 1.76. The PPG with M_W = 18.2 kg/mol and PDI = 1.03 is from Bayer Co. The PVAc/SiO_2 with different loadings was prepared by solution casting[25] in methyl ether ketone (MEK, Sigma-Aldrich). First, a parent PVAc/MEK solution of 0.01 g/mL was prepared and filtered by a poly(tetrafluoroethylene) filter with the pore size of 20 μm to remove impurities and dust. For each sample, 30 mL of the parent solution was transferred into a 100 mL beaker. Then, different amounts of the SiO_2/MEK suspension were added dropwise into the beaker to the desired loading of nanoparticles. After 2 h of stirring, the PVAc/SiO_2/MEK mixture was transferred into a Teflon dish and placed under a fume hood at 293 K for 24 h before drying in a vacuum oven (10^{-2} torr) at 353 K. The PPG/SiO_2 nanocomposite was prepared in a similar manner by replacing the solvent of MEK with ethanol (200 proof, ACS grade, Sigma-Aldrich). The loading of nanoparticles, φ_{NP} (volume fraction), varies from 5 to 40% for PVAc/SiO_2 and φ_{NP} = 38% for PPG/SiO_2 nanocomposite. For the simplicity of the presentation, we will, hereafter, use the name of the parent polymer, the radius of nanoparticle, and the volume fraction of the nanoparticles to represent the nanocomposites. For example, PVAcR7-5.7% refers to PVAc/SiO_2 (R_{NP} = 7 ± 2 nm) nanocomposites with the volume fraction φ_{NP} = 5.7%. A summary of the sample list and basic characterizations is presented in Table 1, where d_{IPS} is the average interparticle surface-to-surface distance (defined in a following section), and R_g is the radius of gyration of the matrix polymer.

Table 1. Basic Characteristics of PNCs

sample name	polymer matrix	R_{NP} (nm)	φ_{NP} (vol %)	d_{IPS} (nm)	d_{IPS}/R_g
PVAcR7-5.7%	PVAc	7	5.7	17	3.0
PVAcR7-7.5%	PVAc	7	7.5	14	2.5
PVAcR7-17%	PVAc	7	17	7.5	1.3
PVAcR7-26%	PVAc	7	26	4.9	0.86
PVAcR7-35%	PVAc	7	35	3.0	0.53
PVAcR7-40%	PVAc	7	40	2.3	0.41
PPGR12.5-38%	PPG	12.5	38	4.7	1.07

2.2. Transmission Electron Microscopy. The transmission electron microscopy (TEM) images of PNCs were produced using JEOL 100CX TEM with an accelerating voltage of 120 kV and a beam current of 100 μA. Film slices of PNCs with thicknesses varying between 100 and 150 nm were prepared by microtoming on RMC Boeckeler PowerTome XL with a glass knife at ambient conditions.

2.3. Thermogravimetric analysis. The weight fraction of the SiO_2 nanoparticles of PNCs was identified by thermogravimetric analysis (TGA) (TA Instruments Q50) from 293 to 1073 K under air at a heating rate of 20 K/min. The volume fraction of the nanoparticles, φ_{NP}, was calculated from the mass fraction of the nanoparticles, m_{NP}, the density of the nanoparticles, and the density of polymers, ρ_{PVAc} = 1.19 g/cm^3 and ρ_{PPG} = 1.004 g/cm^3.[26] The characteristic interparticle surface-to-surface distance, d_{IPS}, was estimated by assuming random distribution of nanoparticles:[27]

$$d_{IPS} = \left(\left(\frac{16}{\pi\varphi_{NP}}\right)^{1/3} - 2\right)R_{NP}.$$

2.4. Broadband Dielectric Spectroscopy. BDS measurements were carried out on a Novocontrol Concept-40 system with an Alpha-A impedance analyzer and a Quatro Cryosystem temperature controller over a frequency range of 10^7 to 10^{-2} Hz. The accuracy of the temperature controller is ±0.1 K. The measurements were performed on a disk-shaped sample sandwiched by two gold electrodes. The sample thickness was 0.15 mm, and the diameter was 14 mm. The BDS tests were performed from T = 393 K to T = 173 K under cooling every 5 K and from 173 to 393 K under heating every 20 K. A thermal annealing of 20 min was performed to assure the thermal equilibrium of the PNCs before each measurement.

2.5. Rheology. All the rheological measurements of PNCs were conducted on an Anton Paar MCR302 on a pair of parallel plates with 4 mm in diameter, except for the neat PVAc, the neat PPG, and the PPGR12.5-38%, where parallel plates with a diameter of 8 mm were applied. All sample thicknesses were 1 mm. To remove the potential effect of sample loading, an oscillatory shear at an amplitude of 30% was applied immediately after the loading.[28,29] Strain sweep tests were conducted at an angular frequency of 1 rad/s at each temperature to identify the linear response region. The applied strain in SAOS varied from 0.01 to 1%, depending on the stiffness of the materials and the measuring temperature. The SAOS measurements were carried out at the angular frequency 10^2 to 10^{-2} rad/s between 313 and 393 K for the PVAc nanocomposites. For the creep compliance measurement, a constant stress of $\sigma \leq 1000$ Pa was applied and the creep measurement lasted for 10^3 to 10^5 s.

3. RESULTS AND DISCUSSION

3.1. Transmission Electron Microscopy. TEM has been widely applied to study the dispersion of the nanoparticles of PNCs.[16,30−32] Figure 1a shows the TEM image of the bulk PVAcR7-26% over a field of view of 1.9 μm × 1.5 μm. Such TEM images with a large field of view should be representative in characterizing the dispersion state of the nanoparticles. Clearly, there are no large nanoparticle aggregates and clusters in the TEM image. To further quantify the dispersion state of the nanoparticles, we calculate the particle−particle pair correlation function, $C(r)$, in ImageJ software by following a previous protocol[30,31] with a background noise tolerance of 10% (Figure 1b). The absence of oscillations in $C(r)$ at r > 20 nm indicates a good dispersion of nanoparticles in the polymer matrix. In addition, we identify the position of each nanoparticle and count the nanoparticle center-to-center distance, $N(l)$ (total counts) (Figure 1c) with l the center-to-center distance of neighboring nanoparticles. The inset of Figure 1c shows a triangle algorithm mapping of the nanoparticles of Figure 1a, and the l is the length of each triangle side. The $N(l)$ follows normal distribution (the solid line in Figure 1c). Note that only the region of the red square box of Figure 1a has been analyzed for Figure 1b,c because of the influence of the scale bar to the image analysis. The detailed analyses of the TEM image over a region larger than the 1.5 μm × 1.5 μm and the optical clarity of the nanocomposites (Figure 1d) are consistent with our previous TEM and small-angle X-ray scattering (SAXS) measurements on the same PVAc/SiO_2 nanocomposites with slightly larger nanoparticle sizes of R_{NP} = 12.5 nm.[13,33] Because of the low glass transition temperature, T_g, of the PPGR12.5-38%, we

DOI: 10.1021/acs.macromol.9b01584
Macromolecules 2020, 53, 302−311

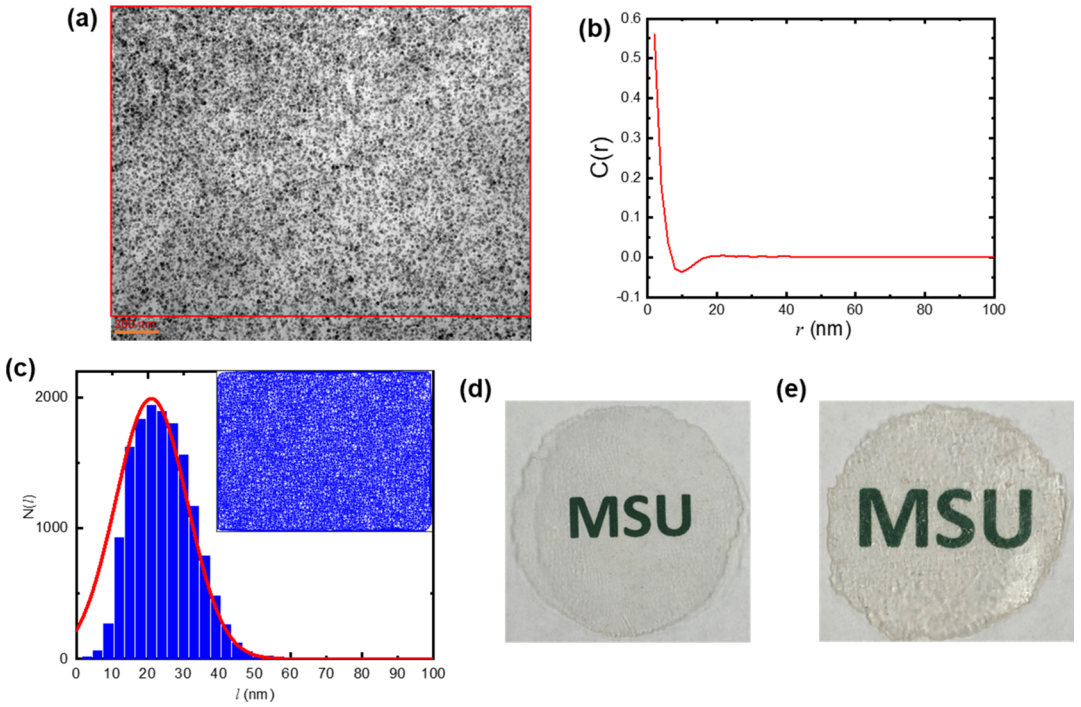

Figure 1. (a) TEM image of PVAcR7-26% over a field of view of 1.9 μm × 1.5 μm. The orange scale bar is 200 nm. (b) Particle−particle pair correlation function, $C(r)$, of the TEM image. (c) Nanoparticle−nanoparticle center-to-center distance distribution, $N(l)$, of the TEM image. The inset of (c) is the triangle algorithm mapping of the nanoparticles in the TEM image. (d,e) Optical images of the bulk PVAcR7-40% (thickness 0.2 mm) and PPGR12.5-38% (thickness 0.4 mm). Note that only the region of the red square box of (a) has been analyzed for (b,c) because of the influence of the scale bar. Both the analyses of the $C(r)$ and the $N(l)$ support a random distribution of nanoparticles in the PNCs. The optical transparency of both samples agrees with the absence of large nanoparticle aggregates of the PNCs.

were not able to microtome the PPG nanocomposite. However, our previous SAXS measurements of PPG/SiO_2 nanocomposite with a lower polymer M_W (M_W = 4 kg/mol) and the same nanoparticles[13] as well as the optical clarity (Figure 1e) of the PPGR12.5-38% favor a good dispersion of silica nanoparticles in the PPGR12.5-38%.

3.2. Broadband Dielectric Spectroscopy. BDS measures the dipole reorientation of the polymer and has been widely applied to study the polymer dynamics of the PNCs.[12,15,34−38] Because the silica nanoparticles do not have an active dipole within the temperature and frequency range of interest, the dielectric spectra of PNCs mainly measure the polymer dynamics.[12,38] Figure 2a shows the typical dielectric loss spectra, $\varepsilon''(\omega)$, of the neat PVAc and PVAc nanocomposites at T = 373 K. The loss peak at 10^6 to 10^7 rad/s represents the segmental relaxation. Adding nanoparticles changes the dielectric spectra of polymer matrix in several ways:[13,14,25,39] (i) the dielectric loss peak shifts to a slightly lower frequency; (ii) the shape of the dielectric loss peak broadens because of the presence of the interfacial polymer layer between the polymer matrix and the nanoparticles; and (iii) an increase in the dc-conductivity occurs, primarily because of the impurities introduced along with the nanoparticles. An accurate analysis on the details of the dielectric spectra of PNCs is generally a challenging task. Recent progress on this topic has been summarized in our previous publications.[14,39] However, because the shape of dielectric loss peak of PNCs remains almost unchanged with temperature (inset Figure 2b), and the focus of the study is on the temperature variations of the polymer dynamics, we take the temperature dependence of the characteristic peak as an indication of the variation of the polymer dynamics with respect to temperature. Specifically, we fit the loss peak into one Havriliak−Negami (HN) equation, $\varepsilon''(\omega) = -\mathrm{Im}\left[\frac{\Delta\varepsilon}{(1+(i\omega\tau_{HN})^{\beta})^{\gamma}} + \frac{\sigma_{dc}}{i\omega\varepsilon_0}\right]$. Here, $\Delta\varepsilon$ is the dielectric strength of the segmental relaxation process, τ_{HN} is the HN relaxation time, the exponents β and γ describe the asymmetry of the spectra, σ_{dc} is the dc-conductivity of the polymer, and ε_0 is the vacuum permittivity. The relationship between the structural relaxation time, τ_α, and τ_{HN} is $\tau_\alpha = \tau_{HN}\left[\sin\frac{\beta\pi}{2+2\gamma}\right]^{-1/\beta}\left[\sin\frac{\beta\gamma\pi}{2+2\gamma}\right]^{1/\beta}$.[40] The dashed lines in Figure 2a are the representations of the HN function fit to the spectra of PVAc PNCs at T = 373 K. Figure 2b summarizes the segmental dynamics of PNCs with temperature. Interestingly, only a slight difference in τ_α has been found between PNCs and the neat polymer. In the inset of Figure 2b, the spectra at different temperatures were normalized by their corresponding peak frequency, ω_p, and the peak amplitude, ε''_p, of the segmental relaxation to compare the shape of the spectra.

In addition to the segmental relaxation, BDS can study the chain relaxation of polymers, which provides a direct comparison to rheology.[41] Figure 2c offers representative dielectric spectra of PPGR12.5-38% (blue squares) and the neat PPG (red circles) at T = 238 K. Both the segmental and chain relaxations of PPG are clearly identified in the loss spectra as well as the derivative spectra of the storage permittivity, $\varepsilon'_{der}(\omega) = -\frac{\pi}{2}\frac{\partial\varepsilon'(\omega)}{\partial\ln\omega}$.[42] The dashed lines are the HN function fit of the segmental relaxation (the long-dashed lines) and the chain relaxation (the short-dashed lines). The inset of Figure 2d presents the normalized spectra, $\varepsilon''/\varepsilon''_p$ versus ω/ω_p, of the PPGR12.5-38% at three temperatures T =

DOI: 10.1021/acs.macromol.9b01584
Macromolecules 2020, 53, 302−311

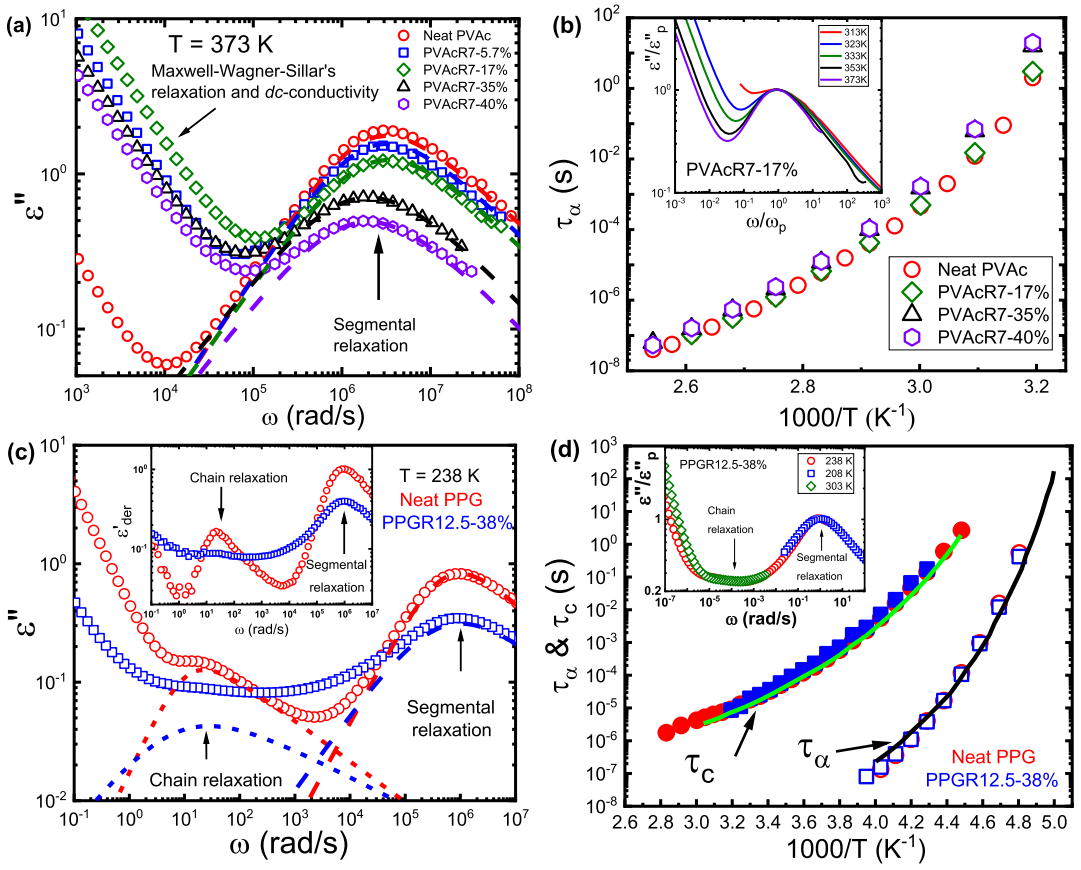

Figure 2. (a) Dielectric loss permittivity spectra, $\varepsilon''(\omega)$, of PVAc nanocomposites and neat PVAc at T = 373 K. (b) Segmental relaxation time, τ_α, of PVAc nanocomposites. (c) $\varepsilon''(\omega)$ of neat PPG and PPGR12.5-38% at T = 238 K. The inset shows their corresponding derivative spectra, $\varepsilon'_{der} = -\frac{\pi}{2} \times \frac{\partial \ln \varepsilon'(\omega)}{\partial \ln \omega}$, where the segmental relaxation and the chain relaxation are well-resolved. (d) Segmental relaxation, τ_α, and the chain relaxation, τ_c, of neat PPG and PPGR12.5-38%. The solid lines in (d) are the τ_α and τ_c of the same PPG from ref 43. The dashed lines in (a,c) are the HN function fit to the spectra. The insets of (c,d) are the normalized spectra of the PVAcR7-17% and PPGR12.5-38% at different temperatures, where the frequency and the dielectric amplitude are normalized by the peak frequency, ω_p, and the peak amplitude, ε''_p, respectively. The spectra of the T = 238 K and T = 308 K of PPGR12.5-38% are compared by matching the peak frequency and peak amplitude of the chain relaxation at T = 308 K with the normalized spectra at T = 238 K.

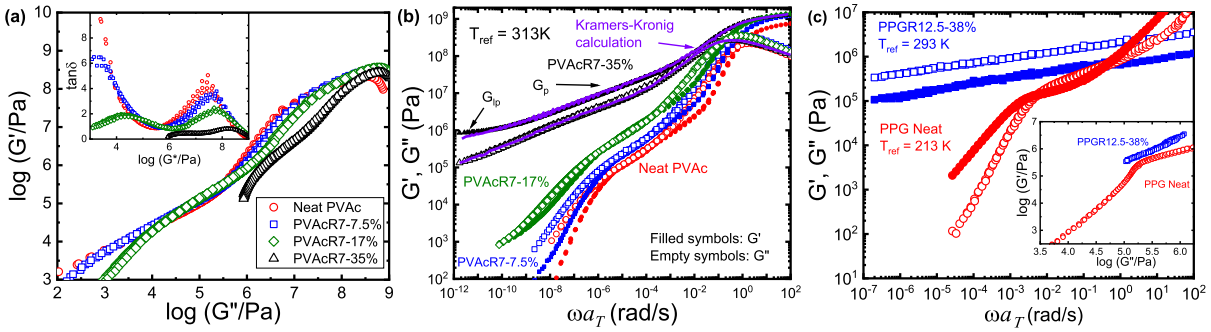

Figure 3. (a) log G' vs log G'' of the PVAc PNCs of different loadings of nanoparticles. The inset presents tan δ vs log G^* of the same PNCs. The good overlap of the spectra at different temperatures indicates the rheological simplicity of the PNCs. Master curves of linear viscoelastic spectra of PVAc PNCs (b) and PPG PNC (c) through TTSP. The reference temperature of PVAc PNCs and the PPG PNC is T_{ref} = 313 K and T_{ref} = 293 K, respectively. The purple lines of (b) are the calculations based on the Kramers−Krönig relation. Both the rubbery plateau, G_p, and the low frequency plateau, G_{lp}, of PVAcR7-35% can be clearly identified from the spectra. The inset of (c) presents the log G' vs log G'' of the neat PPG and the PPGR12.5-38%.

208 K (blue squares), 238 K (red circles), and 308 K (olive diamonds). At T = 308 K, the segmental relaxation peak is outside the frequency window of the measurement, and we match the peak position of chain relaxation at T = 308 K and T = 238 K to compare their shapes. Clearly, except for a slight variation in the dc-conductivity at high temperatures, the shapes of both segmental and chain relaxations do not change with temperature. Therefore, the temperature variations of the characteristic segmental and chain relaxation times represent the corresponding polymer dynamics of PNCs. Figure 2d

DOI: 10.1021/acs.macromol.9b01584
Macromolecules 2020, 53, 302−311

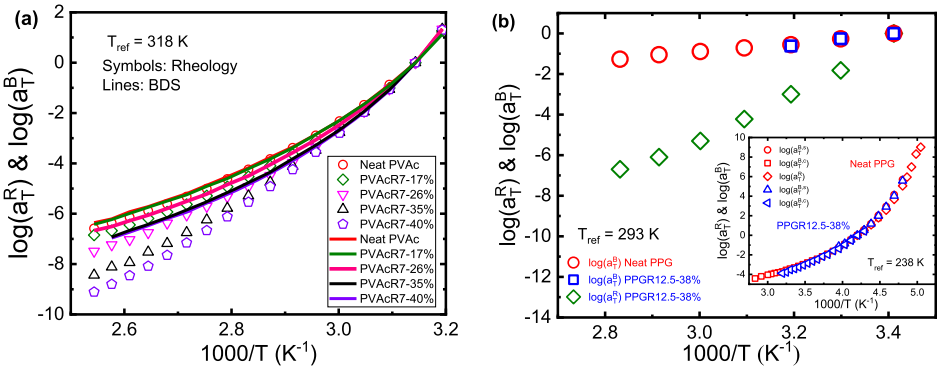

Figure 4. Shift factors of neat PVAc and PVAc PNCs (a) as well as neat PPG and PPGR12.5-38% (b) from rheology $\log(a_T^R)$ and from dielectric $\log(a_T^B)$. The reference temperatures of PVAc PNCs and PPGR12.5-38% are T_{ref} = 318 and 293 K, respectively. The inset of (b) shows the comparison of shift factors of neat PPG and PPG PNC at T_{ref} = 238 K. The excellent overlaps among the $\log(a_T^R)$, $\log(a_T^{B,s})$, and $\log(a_T^{B,c})$ indicate identical temperature dependence of them for neat PPG (red symbols) and PPG nanocomposite (blue symbols) over the whole temperature range of the measurement. Note that the $\log(a_T^R)$ of the PPGR12.5-38% has not been presented in the inset (b).

summarizes the segmental relaxation time, τ_α, and the chain relaxation time, τ_c, of both the PNC and the neat PPG, which are consistent with previous publication on the neat PPG with the same M_W (the solid lines).[43] Interestingly, although the chain relaxation peak broadens significantly, the presence of nanoparticles shows almost no influence on the characteristic time of the chain relaxation.[37] The temperature dependence of both segmental relaxation and chain relaxation of the polymer matrix on PNCs remains identical to that of the neat polymer. Therefore, the BDS measurements clearly demonstrate that the dynamics of polymer matrix of PNCs share almost identical temperature dependence with the neat polymer at both the segmental and the chain level.

3.3. Small Amplitude Oscillatory Shear. Rheology has been heavily applied to study the dynamics of PNCs through the TTSP.[6,9,11] However, the validation of the TTSP for PNCs has not been rigorously examined. Figure 3a and the inset of Figure 3c show log G' versus log G'' of PVAc nanocomposites and the PPG nanocomposite as well as their neat polymer matrices. Master curves of the log G' versus log G'' of all PNCs have been obtained, indicating the rheological simplicity of all PNCs.[44] The inset of Figure 3a presents the Van Gurp–Palmen plot of PVAc nanocomposites with tan δ versus log G^*.[45] Here, G^* is the complex modulus of PNCs with $G^* = \sqrt{G'^2 + G''^2}$. A good overlap of tan δ versus log G^* has been obtained for all the PNCs as well. Figure 3b,c presents the linear viscoelastic master curves of the PNCs through the TTSP at a reference temperature T_{ref} = 313 K for PVAc PNCs and T_{ref} = 293 K for PPG PNC. Indeed, master curves of the PNCs obey the Kramers–Krönig relation[46] as evidenced by the purple lines for the PVAcR7-35% in Figure 3b, where the storage modulus $G'(\omega)$ is calculated from the loss modulus $G''(\omega)$: $G'(\omega) = \frac{2}{\pi}\int_0^\infty \frac{\omega' G''(\omega')}{\omega'^2 - \omega^2} d\omega' + G_0$ with G_0 being a modulus constant, corresponding to the glassy shear modulus.

Several features are worth noting. At low nanoparticle loadings, $\varphi_{NP} \leq 7.5\%$, the PNCs have around 1–2 times higher plateau modulus than the neat polymer, suggesting a slightly stronger effect than pure hydrodynamic reinforcement. An upturn of the $G'(\omega)$ at the terminal region appears at φ_{NP} = 7.5%, which might be from the long relaxation time of the adsorbed polymers. No sign of polymer bridges and the nanoparticle network through bridges has been found for PNCs with $\varphi_{NP} \leq$ 7.5 vol %. Increasing the nanoparticle loading usually leads to an increase in the probabilities for polymer bridging. According to Guiselin,[47] the height of the adsorbed polymers is around R_g of the polymer matrix. Therefore, the nanoparticle network of PNCs with strong polymer bridges shall be anticipated at $d_{IPS}/R_g \approx 1.0$. Indeed, a second modulus plateau, G_{lp}, appears at the frequencies $\omega a_T < 10^{-10}$ rad/s of PVAcR7-17% (d_{IPS}/R_g = 1.3) in addition to the rubbery plateau, G_p, at $\omega a_T = 10^{-7}$ to 10^{-4} rad/s, indicating the emergence of a strong nanoparticle network. Further increasing the loading of nanoparticles to 35 vol % (d_{IPS}/R_g = 0.53) for PVAc PNCs and 38 vol % for PPG PNC significantly improves the dynamic moduli of PNCs. All these features are typical and are consistent with previous literature reports on the characteristics of PNCs.[10]

3.4. Shift Factors of PNCs from Rheology and the Dielectric Measurements. Both rheology and BDS offer the temperature variations of the polymer dynamics of PNCs, manifested by the shift factors a_T^R and a_T^B. BDS offers two distinct types of shift factors: $a_T^{B,s} = \tau_\alpha(T)/\tau_\alpha(T_{ref})$ of segmental relaxation and $a_T^{B,c} = \tau_c(T)/\tau_c(T_{ref})$ of chain relaxation. Although the decoupling of $a_T^{B,s}$ and $a_T^{B,c}$ is well-known in polymers at temperatures close to their T_g,[48] previous experiments showed that the decoupling for PPG took place at temperature T < 222 K.[49] At temperatures above T = 222 K, the shift factors of the $a_T^{B,s}$ and $a_T^{B,c}$ of PPG fall onto one master curve as shown in the inset of Figure 4b, which essentially represents the shift factor of the segmental relaxation of the PPG over the entire temperature window. Thus, we assign $a_T^{B,s}$ as a_T^B for PVAc, and the combination of the $a_T^{B,s}$ and $a_T^{B,c}$ as a_T^B for PPG in the following discussions where the shift factor of segmental relaxation is relevant.

Figure 4a,b shows the explicit temperature dependence of the a_T^R and a_T^B of PVAc nanocomposites and the PPG nanocomposite, respectively. For PNCs with inorganic nanoparticles, the temperature variations in the dynamics should be governed by the polymer matrix. Therefore, one should anticipate identical a_T^R and a_T^B for PNCs as in the neat polymer. However, the comparisons for both PVAc nanocomposites and the PPG nanocomposite show strong deviations between the a_T^R and a_T^B, especially at high loadings. For instance, at T = 393 K, the a_T^R of the PVAcR7-40% is around 100 times smaller than the a_T^B of the neat polymer, implying a $\sim 10^2$ times faster polymer dynamics from rheology than from dielectric measurements. A similar observation can be noted for

DOI: 10.1021/acs.macromol.9b01584
Macromolecules 2020, 53, 302–311

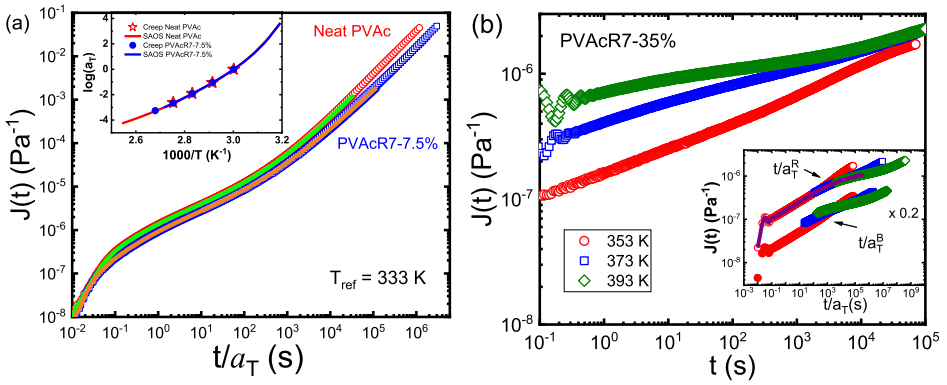

Figure 5. (a) Creep compliance, $J(t)$, of neat PVAc and PVAcR7-7.5% at T_{ref} = 333 K. The lines are the long-time creep of the corresponding samples at T = 333 K. The inset of (a) shows the comparison of the shift factors from SAOS and creep of the neat PVAc and the PVAcR7-7.5%. (b) Creep compliance, $J(t)$, of PVAcR7-35% at T = 353, 373, and 393 K up to 10^5 s. The inset shows the $J(t)$ shifted either by a_T^R or by a_T^B. We multipled the data shifted by a_T^B with a factor of 0.2 for clarity of the presentation. No master curves can be constructed, indicating a failure of the TTSP for PVAcR7-35%. The purple line in the inset (b) is the master curve of $J(t < 100$ s) of PVAcR7-35% at T_{ref} = 353 K.

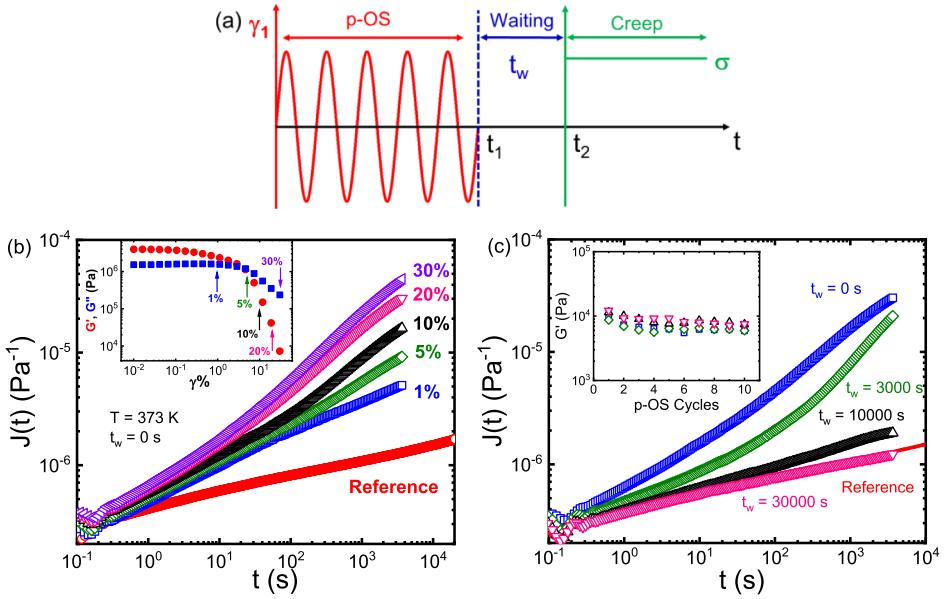

Figure 6. (a) Sketch of the experimental protocol for predeformation treatment followed by creep to decouple the dynamics of the polymer matrix and the nanoparticle network. (b) $J(t)$ of PVAcR7-35% at different predeformation strain amplitudes. The inset of (b) shows the strain sweep that helps to identify the critical strain for the nanoparticle network destruction. (c) $J(t)$ of PVAcR7-35% with a different amount of waiting time. A long waiting time of around 30 000 s is required to obtain a full recovery. The inset is the apparent storage modulus G' at each cycle of the p-OS. The almost identical values for different runs indicate a similar network structure of PNCs after p-OS.

PPGR12.5-38% at T = 353 K, where a ~10^5 faster polymer dynamics has been observed from rheology than from the BDS. More important, if one compares the polymer dynamics of the PNCs with the neat polymer matrix at the same conditions, the same fast dynamic of polymer matrix in PNCs has been observed, which contradicts with the strong attractive polymer−nanoparticle interaction of PNCs. Therefore, the large difference in the a_T^R and a_T^B must be because of different origins. In addition, we find that the a_T^R and a_T^B are almost identical for PVAc PNCs at low loadings with φ_{NP} = 5.7%, 7.5 vol %, and the neat PVAc. In other words, the difference in the temperature dependences of the a_T^R and a_T^B appears only at high loadings with φ_{NP} > 17%. We will discuss the origin of the a_T^R and a_T^B as well as the loading dependence in a later section.

3.5. Creep and the Validation of the TTSP in PNCs. The different temperature dependences of the a_T^R and a_T^B impose an important question on the validation of the TTSP in the PNCs. One possibility is the limited dynamic window (10^{-2} to 10^2 rad/s) of the SAOS measurements. Interestingly, both the log G' versus log G'' and Van Gurp−Palmen plot (Figure 2a) as well as the causality check from the Kramers−Krönig relation (Figure 2b) do not find an obvious sign of the breakdown of the TTSP in PNCs.

Creep is able to access polymer dynamics at the long time limit, which offers a direct way of examining the validation of the TTSP in PNCs. Figure 5a shows the master curves of the creep compliance, $J(t)$, of PNCs for neat PVAc and PVAcR7-7.5%, where the creep compliance across seven decades (10^{-2} to 10^5 s) has been measured at T_{ref} = 333 K. The creep compliance of the PNCs below 7.5% overlaps nicely with each other at different temperatures in the absence of vertical shifts. In addition, the shift factors from the creep are identical to those of the SAOS for both the neat PVAc and the PVAcR7-

DOI: 10.1021/acs.macromol.9b01584
Macromolecules 2020, 53, 302−311

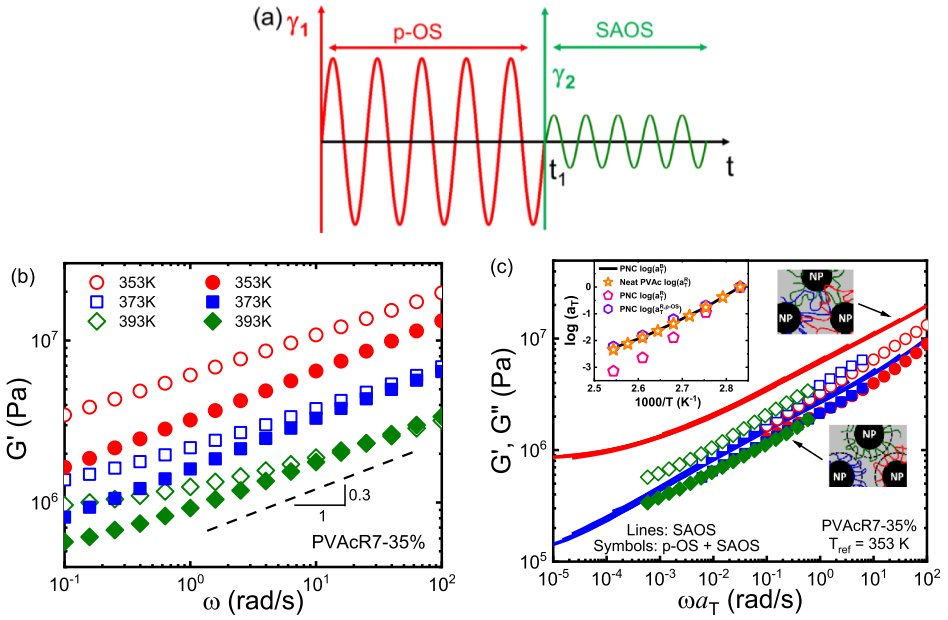

Figure 7. (a) Sketch of the experimental protocol for predeformation treatment followed by SAOS to probe the polymer matrix dynamics after destruction of the nanoparticle network. (b) Linear viscoelastic spectra of PVAcR7-35% before (open symbols) and after (filled symbols) p-OS at T = 353, 373, and 393 K. (c) Master curves of PVAcR7-35% before (solid lines) and after (open circles) p-OS at a reference temperature of 353 K. The inset of (c) shows the comparison of shift factors for neat PVAc and PVAcR7-35% among the $\log(a_T^R)$, $\log(a_T^B)$, and $\log(a_T^{R,p\text{-}OS})$. The identical values of $\log(a_T^{R,p\text{-}OS})$ of PVAcR7-35% and $\log(a_T^R)$ of neat PVAc indicate that the polymer matrix dynamics follow the same temperature dependence as the neat polymer. The cartoon in the inset (c) presents a sketch on the polymer bridge network and the dense colloidal packing of polymer-adsorbed nanoparticles before and after predeformation. The chains are colored for presentation purposes and they have identical polymer chemistry as the matrix polymer (the grey background).

7.5% (the inset of Figure 5a), indicating the validation of the TTSP for PNCs at $\varphi_{NP} \leq 7.5\%$.

Figure 5b shows $J(t)$ of PVAcR7-35% at T = 353, 373, and 393 K. Intriguingly, the shape of the creep compliance of PNCs varies dramatically at different temperatures, especially at 10^2 to 10^5 s outside the accessible time window of the SAOS measurements. Consequently, the creep compliance at different temperatures cannot overlap with each other (the inset of Figure 5b), regardless of the applied shift factors (a_T^R and a_T^B). Thus, the TTSP breaks down for PNCs with high loadings φ_{NP} = 35 vol %. It is worth noting that if one only focuses on the short time dynamics (<10^2 s), a master curve of $J(t = t < 10^2$ s) can be constructed (the purple line in the inset of Figure 5b), with shift factors identical to a_T^R.[9,11] Therefore, the SAOS only observed an "apparent" validation of the TTSP because of the limited dynamic window.

3.6. Dynamics of the Polymer Matrix of PNCs.

3.6.1. Decouple the Dynamics of the Polymer Matrix and the Nanoparticle Network through Predeformation. The mechanics of the nanoparticle network are highly nonlinear with deformation, a phenomenon known as Payne effect.[50] In the Payne effect, a maximum in loss modulus appears at a critical strain, γ_c, beyond which the nanoparticle network decomposes.[51] Therefore, applying predeformation $\gamma > \gamma_c$ followed by linear viscoelastic measurements could separate the contribution of the polymer matrix and the nanoparticle network. Figure 6a shows a sketch of a combination of a predeformation of oscillatory shear (p-OS) with $\gamma_1 > \gamma_c$ followed by a creep test, where $t_w = t_2 - t_1$ is the waiting time, and t_1 and t_2 are the time associated with the end point of p-OS and the starting point of the creep at stress σ. The p-OS runs 10 cycles for all the measurements at an angular frequency of 1 rad/s. In creep experiments, the σ was set as 10^3 Pa to assure a linear response. In the following discussions, we focused on PVAcR7-35%. The underlying physics should apply for other PNCs.

Figure 6b shows the effect of the amplitude γ_1 ($\gamma_1 \geq \gamma_c$) on the creep tests of PNCs with t_w = 0 s, where the γ_c = 1% is located at the loss peak $G''(\gamma)$ in a strain sweep test (the inset of Figure 6b). The destruction of the nanoparticle network takes place at $\gamma > \gamma_c$. Consequently, the $J(t)$ softens significantly upon p-OS. At γ_1 = 1%, there is already three times increase in the $J(t)$ of PNCs. The larger the γ_1, the greater the softening effect and the stronger the disturbance to the nanoparticle network. At γ_1 = 30%, the $J(t)$ increases more than one decade, suggesting a strong destruction of the nanoparticle network. Note that no softening in $J(t)$ has been found after p-OS with γ_1 = 30% in both the neat PVAc and the PVAcR7-7.5%, where no nanoparticle networks present. The softening of PNCs upon deformation has been observed in filled rubbers, where the origin is explained as the destruction of the filler−filler physical network.[6,28,52] We emphasize that the observed softening of PNCs with well-dispersed nanoparticles should be from the destruction of the polymer bridge networks.

To quantify the possible microstructure changes of the nanoparticle network upon p-OS, we further performed experiments with different waiting time, t_w. To assure the PNC resides on a similar rheological state before and after the p-OS, we track the apparent storage modulus, $G'_{p\text{-}OS}(\omega)$, at each circle (the inset of Figure 6c). The nearly identical $G'_{p\text{-}OS}(\omega)$ at each run indicates a similar destruction state of the nanoparticle network of the PNC before applying different t_w. The red line in Figure 6c presents the $J(t)$ of PVAcR7-35% in the absence of p-OS, and the symbols in Figure 6c are the $J(t)$ at t_w = 0−30 000 s with the treatment of p-OS at γ_1 = 20% and

DOI: 10.1021/acs.macromol.9b01584
Macromolecules 2020, 53, 302−311

1 rad/s. As expected, the $J(t)$ decreases with t_w, indicating a healing of the PNC. Remarkably, it takes ~30 000 s before PVAcR7-35% at T = 373 K reaches a completely healed state, which is ~10^{10} τ_α. Recent experiments show that adsorbed polymers take around 10^{10} to 10^{12} τ_α to reach a conformational equilibrium state.[53,54] The coincidence on the time scale between the PNC healing and the equilibrium time of the adsorbed polymers may indicate the reconstruction of the nanoparticle network through a conformation rearrangement of the adsorbed polymers. Nevertheless, the destruction of the network upon predeformation is reversible.

3.6.2. Origin of the Breakdown of the TTSP in PNCs. In this sub-section, we apply a SAOS measurement after the predeformation to study the dynamics of the polymer matrix of PNCs alone. As shown in Figure 7a, the γ_1 and γ_2 are the strain amplitude of the p-OS and the SAOS, respectively. The t_1 is the time of the p-OS. Here, we chose the same p-OS conditions (γ_1 = 20% and ω = 1 rad/s) as in Section 3.6.1.

The empty and filled symbols in Figure 7b are the storage modulus, G', of the PVAcR7-35% before and after p-OS at T = 353, 373, and 393 K. An around 50% reduction in modulus has been found for all temperatures. Figure 7c shows the master curves (symbols) of PVAcR7-35% after p-OS. The shift is obtained based on the horizontal shift in the loss modulus, $G''(\omega)$. In comparison to the master curve of PVAcR7-35% in the absence of the p-OS (the lines), the PNC with p-OS treatment exhibits a power-law behavior, $G'(\omega) \approx G''(\omega) \approx \omega^{0.3}$, and the modulus plateau at low frequencies disappears. The power law of $G'(\omega) \approx G''(\omega) \approx \omega^{0.3}$ is reminiscent of the typical dynamics of dense colloidal systems.[55−58] It is possible that the p-OS breaks up the nanoparticle network, leaving a densely packed polymer adsorbed nanoparticles (the inset cartoons of Figure 7c). Interestingly, the shift factors of the PVAcR7-35% after predeformation (the purple hexagons), $a_T^{R_{p\text{-}OS}}$, are almost identical to the a_T^R of the neat PVAc (the orange stars) and are consistent with the dielectric measurement (a_T^B) of the same PNC (the black line), as shown in the inset of Figure 7c. Therefore, the a_T^R of PNCs contains the contributions from both the polymer matrix and the nanoparticle network that exhibits different temperature variations. Clearly, it is the dynamics of the nanoparticle network that lead to the large difference between the a_T^R and the a_T^B, and the breakdown of the TTSP in PNCs. Note that the nanoparticle network emerges at φ_{NP} = 17% for the PVAc nanocomposites under study, below which the TTSP holds (Figure 5a), which also explains the above-mentioned loading effect for the deviation of the a_T^B and a_T^R (Figure 4a).

3.7. Dynamics and Mechanics of the Nanoparticle Network of PNCs. In PNCs with well-dispersed nanoparticles, a nanoparticle network forms through polymer bridges beyond the gelation. The dynamics of the polymer network is primarily controlled by the polymer desorption, which is an activation process.[59,60] Assuming that the activation energy for polymer desorption is ΔE per chain, the relaxation time of an adsorbed polymer chain is $\tau_{ad}(T) \approx \tau_\alpha(T)\exp\left(\frac{\Delta E}{RT}\right)$,[59] where R = 8.314 J/(mol·K) is the gas constant. Thus, the shift factors of PNCs from rheology, a_T^R, reflect the temperature dependence of the $\tau_{ad}(T)$: $a_T^R = \frac{\tau_c(T)}{\tau_c(T_{ref})} = \frac{\tau_\alpha(T)\exp\left(\frac{\Delta E}{RT}\right)}{\tau_\alpha(T_{ref})\exp\left(\frac{\Delta E}{RT_{ref}}\right)} = a_T^B \exp\left(\frac{\Delta E}{RT} - \frac{\Delta E}{RT_{ref}}\right)$. Therefore, the analyses predict an Arrhenius temperature dependence of the ratio a_T^R/a_T^B with ΔE the energy barrier, in excellent agreement with the experimental observation shown in the inset of Figure 8a for both the PVAc and PPG PNCs. The slopes of the $\log(a_T^R/a_T^B)$ versus $1000/T$ provide a direct identification of the activation energy ΔE.

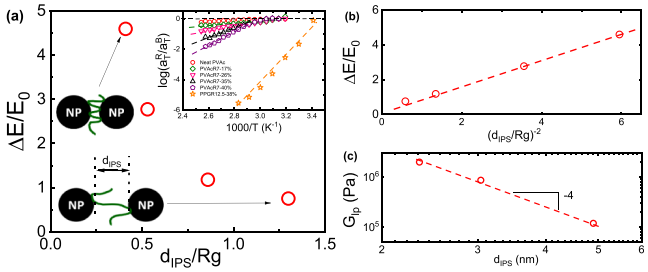

Figure 8. (a) Normalized activation energy, $\Delta E/E_0$, with respect to the normalized interparticle surface-to-surface distance, d_{IPS}/R_g. The inset of (a) demonstrates that the $\log(a_T^R/a_T^B)$ follows an Arrhenius temperature dependence at high temperatures, whose activation energy, ΔE, increases with the nanoparticle loading. The inset cartoon depicts the different scenarios of polymer bridging. (b) $\Delta E/E_0$ in terms of the number density of polymer bridging, $(d_{IPS}/R_g)^{-2}$. (c) Scaling of the low-frequency plateau, G_{lp}, with the d_{IPS}. Both the linear relationship between $\Delta E/E_0$ and $(d_{IPS}/R_g)^{-2}$ and the scaling of $G_{lp} \approx d_{IPS}^{-4}$ confirm the dominating role of the polymer bridges in the dynamics and mechanics of PNCs at high temperatures.

Figure 8a summarizes the $\Delta E/E_0 \approx 0.75-4.5$ with respect to the d_{IPS}/R_g, where the E_0 = 20 kJ/mol is the strength of an H-bonding between PVAc and the SiO_2.[61] The cartoons of Figure 8a illustrate a possible scenario between the d_{IPS}/R_g and the number density of polymer bridges per chain. Interestingly, the activation energy $\Delta E \approx$ 140 kJ/mol of PPGR12.5-38% that is larger than the PVAc PNCs'. Because the E_0 of PPG/SiO_2 and PVAc/SiO_2 is comparable,[61] the larger ΔE of PPGR12.5-38% could be from a larger population of the train conformation at the nanoparticle surfaces of the PPG that is more flexible[13] and has a lower polymer M_W than the PVAc.[62]

According to de Gennes, the number density of bridges between two parallel plates is inversely proportional to the square of the distance.[63] Thus, the number density of polymer bridges of PNCs is $n_b \approx d_{IPS}^{-2}$. Figure 8b plots the number density of H-bonding, $\Delta E/E_0$, as a function of the number density of polymer bridges, $(d_{IPS}/R_g)^{-2}$. Remarkably, a linear relationship has been found between the $\Delta E/E_0$ and $(d_{IPS}/R_g)^{-2}$, supporting the basic ideas of nanoparticle networking through polymer bridges and the bridge desorption controlling the dynamics of nanoparticle network.

For PNCs at high loadings, the desorption energy can be as large as ~90 kJ/mol, and the polymer bridges dominate the elastic contribution of the PNC at high temperatures and at the long-time scale. Therefore, $G_{lp} \approx n_b G_0$, where G_{lp} is the modulus plateau at low frequencies in the linear viscoelastic spectra (Figure 3b), $n_b \approx d_{IPS}^{-2}$ is the number density of the polymer bridge, and $G_0 \approx k_B T/M_x$ is the modulus of one polymer bridge with $M_x \approx d_{IPS}^2$ the M_W of a bridge. The elastic modulus of the nanoparticle network is $G_{lp} \approx n_b G_0 \approx d_{IPS}^{-4}$. Figure 8c plots the G_{lp} versus d_{IPS} for the PVAc nanocomposites. The agreement between experiments and the simple model for the G_{lp} indicates the deterministic role of the polymer bridges for the low-frequency modulus and encourages further experimental verifications.

DOI: 10.1021/acs.macromol.9b01584
Macromolecules 2020, 53, 302−311

4. CONCLUSIONS

In conclusion, we decoupled the dynamics of polymer matrix and the nanoparticle network of PNCs with well-dispersed nanoparticles through a combination of rheology and dielectric spectroscopy. The dielectric measurements show the polymer matrix of PNCs exhibit similar temperature dependence as the neat polymer, regardless of the loading of nanoparticles. The dynamics of PNCs from rheology are comparable to the neat polymer only at nanoparticle loadings in the absence of nanoparticle network, where the shift factors from dielectric measurement and from rheology are similar, and the TTSP is valid. At higher loadings, a nanoparticle network forms through polymer bridging. The shift factors of the PNCs from rheology and from BDS deviate strongly from each other and the TTSP breaks down. In addition, we have demonstrated that predeformation can serve as an effective way to separate the dynamics of polymer matrix and the nanoparticle network. Remarkably, the dynamics of the PNCs from rheology after predeformation exhibit identical shift factors with the dielectric measurements, which indicates a decoupling in the dynamics of polymer matrix from the PNCs. Moreover, it is the emergence of the nanoparticle network that changes the temperature dependence of the dynamics and leads to the breakdown of the TTSP of PNCs. Furthermore, the strength of the nanoparticle network is represented by the strength of polymer bridging. The activation process of the chain desorption at the surface of nanoparticles controls the dynamics of the nanoparticle network. These results provide a detailed characterization of the dynamics of the polymer matrix and the nanoparticle network of PNCs, clarify the decoupling in dynamics of the polymer matrix and the nanoparticle network, and unravel the origin of the breakdown of the TTSP in PNCs.

AUTHOR INFORMATION

Corresponding Authors

*E-mail: weiyang@scu.edu.cn (W.Y.).
*E-mail: chengsh9@msu.edu (S.C.).

ORCID

Wei Yang: 0000-0003-0198-1632
Shiwang Cheng: 0000-0001-7396-4407

Notes

The authors declare no competing financial interest.

ACKNOWLEDGMENTS

S.C. acknowledges financial support from Michigan State University. J.Y. (201706240218) would like to appreciate financial support from the China Scholarship Council during his visit to Michigan State University. W.Y. acknowledges financial support from the National Natural Science Foundation of China (NNSFC grants 51422305 and 51721091).

REFERENCES

(1) Jancar, J.; Douglas, J. F.; Starr, F. W.; Kumar, S. K.; Cassagnau, P.; Lesser, A. J.; Sternstein, S. S.; Buehler, M. J. Current issues in research on structure-property relationships in polymer nanocomposites. *Polymer* **2010**, *51*, 3321−3343.

(2) Kumar, S. K.; Benicewicz, B. C.; Vaia, R. A.; Winey, K. I. 50th Anniversary Perspective: Are Polymer Nanocomposites Practical for Applications? *Macromolecules* **2017**, *50*, 714−731.

(3) Mittal, V.; Kim, J. K.; Pal, K. *Recent Adances in Elastomeric Nanocomposites*; Springer, 2011.

(4) Ray, S. S.; Okamoto, M. Polymer/layered silicate nanocomposites: a review from preparation to processing. *Prog. Polym. Sci.* **2003**, *28*, 1539−1641.

(5) Paul, D. R.; Robeson, L. M. Polymer nanotechnology: Nanocomposites. *Polymer* **2008**, *49*, 3187−3204.

(6) Vilgis, T. A.; Heinrich, G.; Klüppel, M. *Reinforcement of Polymer Nano-Composites: Theory, Experiments and Applications*; Cambridge University Press: Cambridge, 2009.

(7) Kumar, S. K.; Krishnamoorti, R. Nanocomposites: Structure, Phase Behavior, and Properties. *Annu. Rev. Chem. Biomol. Eng.* **2010**, *1*, 37−58.

(8) Kumar, S. K.; Ganesan, V.; Riggleman, R. A. Perspective: Outstanding theoretical questions in polymer-nanoparticle hybrids. *J. Chem. Phys.* **2017**, *147*, 020901.

(9) Mujtaba, A.; Keller, M.; Ilisch, S.; Radusch, H.-J.; Beiner, M.; Thurn-Albrecht, T.; Saalwächter, K. Detection of Surface-Immobilized Components and Their Role in Viscoelastic Reinforcement of Rubber−Silica Nanocomposites. *ACS Macro Lett.* **2014**, *3*, 481−485.

(10) Baeza, G. P.; Dessi, C.; Costanzo, S.; Zhao, D.; Gong, S.; Alegria, A.; Colby, R. H.; Rubinstein, M.; Vlassopoulos, D.; Kumar, S. K. Network dynamics in nanofilled polymers. *Nat. Commun.* **2016**, *7*, 11368.

(11) Lorenz, B.; Pyckhout-Hintzen, W.; Persson, B. N. J. Master curve of viscoelastic solid: Using causality to determine the optimal shifting procedure, and to test the accuracy of measured data. *Polymer* **2014**, *55*, 565−571.

(12) Holt, A. P.; Griffin, P. J.; Bocharova, V.; Agapov, A. L.; Imel, A. E.; Dadmun, M. D.; Sangoro, J. R.; Sokolov, A. P. Dynamics at the Polymer/Nanoparticle Interface in Poly(2-vinylpyridine)/Silica Nanocomposites. *Macromolecules* **2014**, *47*, 1837−1843.

(13) Cheng, S.; Carroll, B.; Lu, W.; Fan, F.; Carrillo, J.-M. Y.; Martin, H.; Holt, A. P.; Kang, N.-G.; Bocharova, V.; Mays, J. W.; Sumpter, B. G.; Dadmun, M.; Sokolov, A. P. Interfacial Properties of Polymer Nanocomposites: Role of Chain Rigidity and Dynamic Heterogeneity Length Scale. *Macromolecules* **2017**, *50*, 2397−2406.

(14) Carroll, B.; Cheng, S.; Sokolov, A. P. Analyzing the Interfacial Layer Properties in Polymer Nanocomposites by Broadband Dielectric Spectroscopy. *Macromolecules* **2017**, *50*, 6149−6163.

(15) Klonos, P.; Panagopoulou, A.; Kyritsis, A.; Bokobza, L.; Pissis, P. Dielectric studies of segmental dynamics in poly(dimethylsiloxane)/titania nanocomposites. *J. Non-Cryst. Solids* **2011**, *357*, 610−614.

(16) Chen, Q.; Gong, S.; Moll, J.; Zhao, D.; Kumar, S. K.; Colby, R. H. Mechanical Reinforcement of Polymer Nanocomposites from Percolation of a Nanoparticle Network. *ACS Macro Lett.* **2015**, *4*, 398−402.

(17) Huber, G.; Vilgis, T. A. On the Mechanism of Hydrodynamic Reinforcement in Elastic Composites. *Macromolecules* **2002**, *35*, 9204−9210.

(18) Zhu, Z.; Thompson, T.; Wang, S.-Q.; von Meerwall, E. D.; Halasa, A. Investigating Linear and Nonlinear Viscoelastic Behavior Using Model Silica-Particle-Filled Polybutadiene. *Macromolecules* **2005**, *38*, 8816−8824.

(19) Sternstein, S. S.; Zhu, A.-J. Reinforcement Mechanism of Nanofilled Polymer Melts As Elucidated by Nonlinear Viscoelastic Behavior. *Macromolecules* **2002**, *35*, 7262−7273.

(20) Wang, Z.; Liu, J.; Wu, S.; Wang, W.; Zhang, L. Novel percolation phenomena and mechanism of strengthening elastomers by nanofillers. *Phys. Chem. Chem. Phys.* **2010**, *12*, 3014−3030.

(21) Wang, M.-J. Effect of Polymer-Filler and Filler-Filler Interactions on Dynamic Properties of Filled Vulcanizates. *Rubber Chem. Technol.* **1998**, *71*, 520−589.

(22) Zhang, Q.; Archer, L. A. Poly(ethylene oxide)/Silica Nanocomposites: Structure and Rheology. *Langmuir* **2002**, *18*, 10435−10442.

DOI: 10.1021/acs.macromol.9b01584
Macromolecules 2020, 53, 302−311

(23) Iijima, M.; Kamiya, H. Layer-by-Layer Surface Modification of Functional Nanoparticles for Dispersion in Organic Solvents. *Langmuir* **2010**, *26*, 17943−17948.
(24) Kamiya, H.; Suzuki, H.; Kato, D.; Jimbo, G. Densification of Alkoxide-Derived Fine Silica Powder Compact by Ultra-High-Pressure Cold Isostatic Pressing. *J. Am. Ceram. Soc.* **1993**, *76*, 54−64.
(25) Cheng, S.; Holt, A. P.; Wang, H.; Fan, F.; Bocharova, V.; Martin, H.; Etampawala, T.; White, B. T.; Saito, T.; Kang, N.-G.; Dadmun, M. D.; Mays, J. W.; Sokolov, A. P. Unexpected Molecular Weight Effect in Polymer Nanocomposites. *Phys. Rev. Lett.* **2016**, *116*, 038302.
(26) Brandrup, J.; Immergut, E. H.; Grulke, E. A. *Polymer Handbook*, 4th ed.; Wiley-Interscience, 2003.
(27) Wu, S. Phase structure and adhesion in polymer blends: A criterion for rubber toughening. *Polymer* **1985**, *26*, 1855−1863.
(28) Wang, X.; Robertson, C. G. Strain-induced nonlinearity of filled rubbers. *Phys. Rev. E: Stat., Nonlinear, Soft Matter Phys.* **2005**, *72*, 031406.
(29) Li, S.; Mi, Y.; Wang, X. Superposed nonlinear rheological behavior in filled elastomers. *J. Rheol.* **2017**, *61*, 409−425.
(30) Jouault, N.; Moll, J. F.; Meng, D.; Windsor, K.; Ramcharan, S.; Kearney, C.; Kumar, S. K. Bound Polymer Layer in Nanocomposites. *ACS Macro Lett.* **2013**, *2*, 371−374.
(31) Jouault, N.; Zhao, D.; Kumar, S. K. Role of Casting Solvent on Nanoparticle Dispersion in Polymer Nanocomposites. *Macromolecules* **2014**, *47*, 5246.
(32) Li, X.; Zhang, H.; Jin, J.; Huang, D.; Qi, X.; Zhang, Z.; Yu, D. Quantifying Dispersion of Nanoparticles in Polymer Nanocomposites Through Transmission Electron Microscopy Micrographs. *J. Micro Nano-Manufacturing* **2014**, *2*, 021008.
(33) Cheng, S.; Bocharova, V.; Belianinov, A.; Xiong, S.; Kisliuk, A.; Somnath, S.; Holt, A. P.; Ovchinnikova, O. S.; Jesse, S.; Martin, H.; Etampawala, T.; Dadmun, M.; Sokolov, A. P. Unraveling the Mechanism of Nanoscale Mechanical Reinforcement in Glassy Polymer Nanocomposites. *Nano Lett.* **2016**, *16*, 3630−3637.
(34) Bogoslovov, R. B.; Roland, C. M.; Ellis, A. R.; Randall, A. M.; Robertson, C. G. Effect of Silica Nanoparticles on the Local Segmental Dynamics in Poly(vinyl acetate). *Macromolecules* **2008**, *41*, 1289−1296.
(35) Füllbrandt, M.; Purohit, P. J.; Schönhals, A. Combined FTIR and Dielectric Investigation of Poly(vinyl acetate) Adsorbed on Silica Particles. *Macromolecules* **2013**, *46*, 4626−4632.
(36) Gong, S.; Chen, Q.; Moll, J. F.; Kumar, S. K.; Colby, R. H. Segmental Dynamics of Polymer Melts with Spherical Nanoparticles. *ACS Macro Lett.* **2014**, *3*, 773−777.
(37) Casalini, R.; Roland, C. M. Local and Global Dynamics in Polypropylene Glycol/Silica Composites. *Macromolecules* **2016**, *49*, 3919−3924.
(38) Holt, A. P.; Sangoro, J. R.; Wang, Y.; Agapov, A. L.; Sokolov, A. P. Chain and Segmental Dynamics of Poly(2-vinylpyridine) Nanocomposites. *Macromolecules* **2013**, *46*, 4168−4173.
(39) Cheng, S.; Mirigian, S.; Carrillo, J.-M. Y.; Bocharova, V.; Sumpter, B. G.; Schweizer, K. S.; Sokolov, A. P. Revealing spatially heterogeneous relaxation in a model nanocomposite. *J. Chem. Phys.* **2015**, *143*, 194704.
(40) Kremer, F.; Schohals, A. *Broadband Dielectric Spectroscopy*; Springer-Verlag: Berlin, 2002.
(41) Adachi, K.; Kotaka, T. Dielectric normal mode relaxation. *Prog. Polym. Sci.* **1993**, *18*, 585−622.
(42) Wübbenhorst, M.; van Turnhout, J. Analysis of complex dielectric spectra. I. One-dimensional derivative techniques and three-dimensional modelling. *J. Non-Cryst. Solids* **2002**, *305*, 40−49.
(43) Gainaru, C.; Hiller, W.; Böhmer, R. A Dielectric Study of Oligo- and Poly(propylene glycol). *Macromolecules* **2010**, *43*, 1907−1914.
(44) Dae Han, C.; Kim, J. K. On the use of time-temperature superposition in multicomponent/multiphase polymer systems. *Polymer* **1993**, *34*, 2533−2539.
(45) Van Gurp, M.; Palmen, J. Time-temperature superposition for polymeric blends. *Rheol. Bull.* **1998**, *67*, 5−6.
(46) Ferry, J. D. *Viscoelastic Properties of Polymers*; Wiley: New York, 1980.
(47) Guiselin, O. Irreversible Adsorption of a Concentrated Polymer Solution. *Europhys. Lett.* **1992**, *17*, 225.
(48) Ding, Y.; Sokolov, A. P. Breakdown of time-temperature superposition principle and universality of chain dynamics in polymers. *Macromolecules* **2006**, *39*, 3322−3326.
(49) Schönhals, A.; Schlosser, E. Relationship between segmental and chain dynamics in polymer melts as studied by dielectric spectroscopy. *Phys. Scr.* **1993**, *T49A*, 233−236.
(50) Payne, A. R. The dynamic properties of carbon black-loaded natural rubber vulcanizates. Part I. *J. Appl. Polym. Sci.* **1962**, *6*, 57−63.
(51) Majesté, J.-C.; Vincent, F. A kinetic model for silica-filled rubber reinforcement. *J. Rheol.* **2015**, *59*, 405−427.
(52) Robertson, C. G.; Wang, X. R. Isoenergetic jamming transition in particle-filled systems. *Phys. Rev. Lett.* **2005**, *95*, 075703.
(53) Napolitano, S.; Capponi, S.; Vanroy, B. Glassy dynamics of soft matter under 1D confinement: How irreversible adsorption affects molecular packing, mobility gradients and orientational polarization in thin films. *Eur. Phys. J. E* **2013**, *36*, 61.
(54) Housmans, C.; Sferrazza, M.; Napolitano, S. Kinetics of Irreversible Chain Adsorption. *Macromolecules* **2014**, *47*, 3390−3393.
(55) Sollich, P. Rheological constitutive equation for a model of soft glassy materials. *Phys. Rev. E: Stat. Phys., Plasmas, Fluids, Relat. Interdiscip. Top.* **1998**, *58*, 738−759.
(56) Fielding, S. M.; Sollich, P.; Cates, M. E. Aging and rheology in soft materials. *J. Rheol.* **2000**, *44*, 323−369.
(57) Saltzman, E. J.; Schweizer, K. S. Transport coefficients in glassy colloidal fluids. *J. Chem. Phys.* **2003**, *119*, 1197−1203.
(58) Schweizer, K. S.; Saltzman, E. J. Entropic barriers, activated hopping, and the glass transition in colloidal suspensions. *J. Chem. Phys.* **2003**, *119*, 1181−1196.
(59) Chernyak, Y. B.; Leonov, A. I. On the theory of the adhesive friction of elastomers. *Wear* **1986**, *108*, 105−138.
(60) Sarvestani, A. S.; Picu, C. R. Network model for the viscoelastic behavior of polymer nanocomposites. *Polymer* **2004**, *45*, 7779−7790.
(61) Gilli, G.; Gilli, P. *The Nature of the Hydrogen Bond: Outline of a Comprehensive Hydrogen Bond Theory*, 1st ed.; Oxford University Press, 2009.
(62) Scheutjens, J. M. H. M.; Fleer, G. J. Statistical theory of the adsorption of interacting chain molecules. 2. Train, loop, and tail size distribution. *J. Phys. Chem.* **1980**, *84*, 178−190.
(63) De Gennes, P. G. Polymers at an interface; a simplified view. *Adv. Colloid Interface Sci.* **1987**, *27*, 189−209.

DOI: 10.1021/acs.macromol.9b01584
Macromolecules 2020, 53, 302−311